Published OnlineFirst January 21, 2014; DOI: 10.1158/0008-5472.CAN-13-1012

Cancer Research

Axon Guidance Factor SLIT2 Inhibits Neural Invasion and Metastasis in Pancreatic Cancer

Andreas Göhrig, Katharina M. Detjen, Georg Hilfenhaus, et al.

Cancer Res Published OnlineFirst January 21, 2014.

Published OnlineFirst January 21, 2014; DOI: 10.1158/0008-5472.CAN-13-1012

Tumor and Stem Cell Biology

Cancer Research

Axon Guidance Factor SLIT2 Inhibits Neural Invasion and Metastasis in Pancreatic Cancer

Andreas Göhrig[1,2], Katharina M. Detjen[1,2], Georg Hilfenhaus[2], Jan L. Körner[2], Martina Welzel[1,2], Ruza Arsenic[4], Rosa Schmuck[3], Marcus Bahra[3], Jane Y. Wu[5], Bertram Wiedenmann[2], and Christian Fischer[1,2]

Abstract

Pancreatic ductal adenocarcinoma (PDAC) metastasizes by neural, vascular, and local invasion routes, which limit patient survival. In nerves and vessels, SLIT2 and its ROBO receptors constitute repellent guidance cues that also direct epithelial branching. Thus, the SLIT2–ROBO system may represent a key pinch point to regulate PDAC spread. In this study, we examined the hypothesis that escaping from repellent SLIT2–ROBO signaling is essential to enable PDAC cells to appropriate their local stromal infrastructure for dissemination. Through immunohistochemical analysis, we detected SLIT2 receptors ROBO1 and ROBO4 on epithelia, nerves, and vessels in healthy pancreas and PDAC specimens, respectively. SLIT2 mRNA expression was reduced in PDAC compared with nontransformed pancreatic tissues and cell lines, suggesting a reduction in SLIT2–ROBO pathway activity in PDAC. In support of this interpretation, restoring the SLIT2 expression in SLIT2-deficient PDAC cells inhibited their bidirectional chemoattraction with neural cells, and more specifically, impaired unidirectional PDAC cell navigation along outgrowing neurites in models of neural invasion. Restoring autocrine/paracrine SLIT2 signaling was also sufficient to inhibit the directed motility of PDAC cells, but not their random movement. Conversely, RNA interference–mediated silencing of ROBO1 stimulated the motility of SLIT2-competent PDAC cells. Furthermore, culture supernatants from SLIT2-competent PDAC cells impaired migration of endothelial cells (human umbilical vein endothelial cells), whereas an N-terminal SLIT2 cleavage fragment stimulated such migration. *In vivo* investigations of pancreatic tumors with restored SLIT2 expression demonstrated reduced invasion, metastasis, and vascularization, with opposing effects produced by ROBO1 silencing in tumor cells or sequestration of endogenous SLIT2. Analysis of clinical specimens of PDAC showed that those with low SLIT2 mRNA expression exhibited a higher incidence and a higher fraction of tumor-infiltrated lymph nodes. Taken together, our findings argue that disrupting SLIT2–ROBO signaling in PDAC may enhance metastasis and predispose PDAC cells to neural invasion. *Cancer Res; 74(5); 1–12. ©2014 AACR.*

Introduction

Pancreatic ductal adenocarcinoma (PDAC) is the fourth leading cause of cancer-related deaths in the Western world with a 5-year survival rate of <5% (reviewed in ref. 1). Because of early invasive growth and metastatic spread, the vast majority of patients are diagnosed with advanced, unresectable disease, facing a median survival of 4 to 6 months under palliative chemotherapy (1). Even after curative resection, median survival is as low as 12 to 20 months, as most patients eventually experience disease recurrence (1).

Neural invasion represents a key pathologic feature of PDAC, and a distinct and independent route of tumor cell spread (reviewed in ref. 2). Neural invasion is considered a major risk factor of tumor recurrence and a major cause of neuropathic pain and, hence, limits both the success of curative surgery and the quality of life of patients with PDAC. Neural invasion is currently perceived as a process driven by mutual attraction and reciprocal interaction between tumor cells and nerves, resulting in both, axonal growth and tumor cell invasion (2–4). Thus, neural hypertrophy and increased nerve densities are frequent pathologic features of PDAC, indicating that tumor cells affect neural morphology and plasticity (5). Several signaling molecules from neural and/or tumor cells, have been implicated in neural invasion, including soluble ligands such as neurotrophins, cytokines, and chemokines, as well as cell surface–bound ligands and their respective receptors (2).

Axon guidance factors and their receptors constitute a signaling system with features that uniquely qualify them as

Authors' Affiliations: [1]Experimental and Clinical Research Center, a joint cooperation between the Charité Medical Faculty and the Max-Delbrück Center for Molecular Medicine, Berlin, Germany; [2]Medizinische Klinik mit Schwerpunkt Hepatologie und Gastroenterologie; [3]Klinik für Viszeral-, Allgemein-, und Transplantationschirurgie; [4]Institut für Pathologie, Charité-Universitätsmedizin Berlin, Germany; and [5]Department of Neurology, Lurie Cancer Center, Center for Genetic Medicine, Northwestern University Feinberg School of Medicine

Note: Supplementary data for this article are available at Cancer Research Online (http://cancerres.aacrjournals.org/).

A. Göhrig and K.M. Detjen contributed equally to this work.

Corresponding Author: Christian Fischer, Medizinische Klinik mit Schwerpunkt Hepatologie und Gastroenterologie, Charité-Universitätsmedizin Berlin, Campus Virchow-Klinikum, Augustenburger Platz 1, 13353 Berlin, Germany. Phone: 49-30-450553042; Fax: 49-30-450540937; E-mail: christian.fischer@charite.de

doi: 10.1158/0008-5472.CAN-13-1012

Published OnlineFirst January 21, 2014; DOI: 10.1158/0008-5472.CAN-13-1012

regulators of neural invasion. Physiologically, axon guidance factors function as molecular cues to control growth, navigation, and positioning of neurons in the developing brain (6). Furthermore, blood vessels, which arose later in evolution than nerves, co-opted several of the molecular mechanisms that originally served the nervous system (7). Thus, well-established regulators of angiogenesis, such as VEGF, originated as regulators of neurogenesis; conversely, axon guidance factors act on endothelial cells to control angiogenesis (7). Axon guidance molecules, therefore, represent attractive candidate regulators of both networks that provide the infrastructure for PDAC metastatic spread, i.e., vascular routes and neural invasion.

SLITs and their ROBO receptors are such guidance factors that navigate nerves and vessels (7–9). By now, three mammalian SLIT homologues (SLIT1–3) have been characterized. The activity of secreted SLIT ligands is mediated through interaction with Robos, which are single-pass transmembrane receptors belonging to the immunoglobulin superfamily of cell adhesion molecules (8–10). Originally characterized as repulsive axon guidance cues in midline crossing of commissural axons during neural development (11, 12), subsequent genetic studies confirmed SLITs and ROBOs as chemorepellent cues controlling axon guidance and branching (13), migration of neurons and glia (14, 15), and navigation of neural crest cells during neurogenesis (16, 17). However, SLITs and ROBOs also function in developmental processes outside the nervous system (9, 10). Thus, the discovery of the endothelial specific receptor ROBO4 suggested a key role of the SLIT–ROBO system in angiogenesis (18, 19), and indeed revealed that SLIT2 also regulates angiogenic sprouting and vascular homeostasis (reviewed in refs. 9, 10). In addition, chemorepellent SLIT2 signaling has been implicated in the control of stereotypic and polarized branching morphogenesis during development of epithelial organs such as kidney, mammary gland, and lungs (20–22). The tightly regulated pathways that control morphogenesis are frequently corrupted in epithelial malignancies (9, 10), and SLIT2 has indeed been implicated in a number of human tumors. Initial seminal studies reported overexpression of SLIT2 in human tumor samples and functionally linked SLIT2 with enhanced tumor growth and vascularization (23). However, loss of SLIT2 expression by epigenetic inactivation was reported in tumors such as breast, colon, and lung cancer (24, 25), and low SLIT2 mRNA expression was associated with distant metastasis and poor survival (9, 10). Loss of SLIT2 was, furthermore, linked to aberrant growth and migration of tumor epithelial cells, thereby promoting tumor growth and metastatic spread in experimental settings (9, 10). To date, neither expression nor function of the SLIT2–ROBO system in PDAC has been studied in detail. Therefore, we addressed the function of SLIT2–ROBO guidance cues for growth, metastasis, angiogenesis, and neural invasion of PDAC.

Material and Methods

Materials

Antibodies were from Sigma-Aldrich (Flag), Invitrogen (Myc), Millipore (SLIT2 and cortactin), Bethyl (ROBO1), Abcam (ROBO4), and BD Pharmingen (CD31). Human SLIT2N was from Sigma-Aldrich and PeproTech, and ROBO1-Fc from R&D Systems.

Cell culture

MiaPaCa, ASPC1, and Panc1 cells were from the American Type Culture Collection (ATCC); Capan-1, Capan-2, and DANG cells were from Leibniz Institute DSMZ and maintained as described in ref. 26. The immortal HPDE cell line H6c7 was from the University Health Network (27, 28).

Pancreatic cancer specimens

Tissue samples were from patients with PDAC undergoing surgery at Charité-Universitätsmedizin from 1996 to 2013. Patients gave written informed consent. Data on tumor–node–metastasis (TNM) classification and tumor infiltration of lymph nodes were retrieved from pathology reports.

Quantitative RT-PCR

RNA was purified using the RNeasy Mini Kit (Qiagen), and quantified on Agilent's 2100 Bioanalyzer using the RNA 6000 Nano Kit (Agilent). Quantitative real-time PCR (qRT-PCR) was conducted in triplicate using SLIT2 TaqMan primer/probes (Hs00191193_m1; Applied Biosystems) with the One-Step RT-PCR Kit (Invitrogen) on a CFX96 Touch Real-Time PCR Detection System thermal cycler (Bio-Rad). RNA isolation and qRT-PCR of cultured cells were performed as described in ref. 29. Relative quantification was calculated by the Livak method.

Generation of cell clones

Full-length SLIT2-cDNA (Hs.29802; imaGenes) was flanked by a N-terminal 3xFlag-tag and subcloned into pcDNA4/TO-3xflag-mycHIS (T-REx; Invitrogen), resulting in pcDNA4/TO-SP-3xflag-SLIT2-mycHis. Following sequential transfection of pcDNA6/TR (cells described in ref. 30) and pcDNA4/TO-SP-3xflag-SLIT2-mycHis, SLIT2 expression was induced by 1 μg/mL doxycycline (Sigma-Aldrich). Cells expressing pcDNA6/TR were used to exclude off-target effects of doxycycline. MISSION Lentiviral Transduction Particles (Sigma-Aldrich) for shRNA-mediated ROBO1-knockdown and nontarget control particles were used at a multiplicity of infection (MOI) of 10 and clones were selected with 0.6 μg/mL puromycin.

Preparation of cell extracts and immunoblotting

The 5×10^6 cells were treated with doxycycline for 48 hours, lysed in 100 μL RIPA buffer and immunoblotted as described in ref. 26. Trichloroacetic acid precipitates from culture supernatants were prepared as described in ref. 26.

Migration and invasion assays

For migration assays, 2×10^5 cells per insert (doxycycline-pretreated, if applicable) were placed in serum-free medium in 8 μm Transwell inserts (Corning) and allowed to migrate toward chemotactic gradients for the times indicated. Migrated cells were stained with crystal violet or 4′,6-diamidino-2-phenylindole (DAPI) and quantified by counting five standardized fields at ×100 magnification (29, 31). Please refer to Supplementary Materials and Methods for details. For 3D Matrigel Invasion assays, 8 μm Transwells were coated with

Published OnlineFirst January 21, 2014; DOI: 10.1158/0008-5472.CAN-13-1012

1 mg/mL growth factor–reduced Matrigel (BD Pharmingen). Experiments were performed in triplicates.

Lamellopodia formation of endothelial cells

Serum-starved human umbilical vein endothelial cells (HUVEC; Lonza) were grown on collagen-coated cover slides. Following treatments, cells were fixed with 70% ethanol and costained with phalloidin and fluorescein isothiocyanate (FITC)–conjugated α-cortactin. Lamellopodia were quantified using AxioVision (Zeiss) and ImageJ software (NIH).

Tumor models

Local authorities approved the animal experiments. Female severe combined immunodeficient (SCID) beige mice (20–24) were from Charles River Laboratories. For orthotopic tumors, 10^6 cells were injected into the pancreatic head (26, 29). After 7 (MiaPaCa) or 3 (DANG) weeks, mice were sacrificed, primary tumors harvested, and enlarged lymph nodes were collected. Metastatic nodules in the mesentery were counted as described in ref. 29.

Immunohistochemical analyses

Immunohistochemistry was conducted on cryostat sections as described and the average number of CD31-positive vessels was determined from digital images of three regions of maximal vascular density (MiaPaCa) or by counting of all vessels per field (DANG) at ×100 magnification (26).

Dorsal root ganglia–tumor cell coculture assay

Dorsal root ganglia (DRG) and tumor cells were placed in separate growth factor–reduced Matrigel drops at 1 mm distance in 12-well plates, and connected with a Matrigel bridge. Time-lapse imaging (Leica DMI6000 B) conducted between 9 and 15 days of culture was evaluated using automated acquisition software (Leica LAS AF6000). Images of individual tumor cells were taken every 30 minutes to follow locomotion. Travel distances, velocity, and directness were calculated using ImageJ and ibidi Chemotaxis software (refer to Supplementary Materials and Methods for further details).

Statistical analysis

Statistical significance was determined by the *t* test, Fisher exact test, and Mann–Whitney test using GraphPad Prism. Data represent means ± SEM unless stated otherwise.

Results

SLIT2 mRNA expression is reduced in human PDAC and correlates with lymphatic metastasis

Initial experiments assessed the expression of the SLIT2 receptors ROBO1 and ROBO4 in pancreatic tissues. Immunohistochemistry localized ROBO1 to ductal epithelial cells and ROBO4 to the vasculature of both the nontransformed pancreas and PDAC (Fig. 1A–F). Moreover, ROBO1 immunoreactivity was localized on pancreatic nerves (Fig. 1C), as confirmed by serial sections stained with the neuronal marker S100 (Supplementary Fig. S1A–S1C).

Next, we determined SLIT2 expression in PDAC cell lines and human tissue samples. SLIT2 mRNA was low or absent in all PDAC cell lines examined except the well-differentiated cell line DANG, which exhibited levels comparable with the immortalized pancreatic epithelial cell line HPDE (Fig. 1G). 5-AZA-dC treatment reactivated SLIT2 expression in Panc1 cells (Supplementary Fig. S1D), suggesting epigenetic silencing as one potential mechanism of SLIT2 inactivation. Moreover, qRT-PCR indicated a reduction of SLIT2 mRNA expression in PDAC when compared with nontransformed pancreas in clinical specimens, both in the overall cohort (Fig. 1H) and the subgroup of paired tumor and nontransformed tissues (Supplementary Fig. S1F). On the basis of the best separation indicated in receiver-operator characteristic curves, we identified tumors with pathologic SLIT2 mRNA expression (Fig. 1I). In these tumors, SLIT2 mRNA expression < median correlated with higher incidence (Fig. 1J) and a higher extent of lymph node metastasis (Fig. 1K). Conversely, N1 tumors exhibited lower SLIT2 mRNA than N0 tumors. Thus, the SLIT2–ROBO signaling pathway is present in the pancreas, and SLIT2 expression is reduced in patients with PDAC with nodal metastasis.

SLIT2 inhibits directed migration and invasion of PDAC cells *in vitro*

To experimentally address the function of SLIT2 in PDAC, we decided on tetracycline-inducible reexpression of SLIT2 in MiaPaCa and Panc1 cells, which lack endogenous SLIT2 (Fig. 1G). Doxycycline-induced production and secretion of myc- and Flag-tagged full-length SLIT2, and of the bioactive, ROBO-binding N-terminal cleavage fragment SLIT2N (32) in MiaPaCa$^{TR\text{-}SLIT2}$ and Panc1$^{TR\text{-}SLIT2}$ clones was confirmed by immunoblotting (Fig. 2A and Supplementary Fig. S2A). Thus, transfected PDAC cells produced and processed SLIT2.

As ROBO1 is present on MiaPaCa and Panc1 cells (Supplementary Fig. S1E), we initially determined auto/paracrine SLIT2 effects *in vitro*. SLIT2 reexpression did not affect proliferation of PDAC cells (Fig. 2B and Supplementary Fig. S2B), nor did it affect random migration (Fig. 2C and Supplementary Fig. S3) and wound healing of MiaPaCa$^{TR\text{-}SLIT2}$ monolayers (Fig. 2D). However, SLIT2 induction markedly inhibited directed migration and invasion of MiaPaCa$^{TR\text{-}SLIT2}$ (Fig. 2E and F) and Panc1$^{TR\text{-}SLIT2}$ cells (Supplementary Fig. S2C and S2D). SLIT2 effects on migration were prevented by cotreatment with the soluble ROBO1-decoy receptor ROBON (Fig. 2G). Migration of MiaPaCa and Panc1 clones with stable overexpression of SLIT2 was similarly inhibited by 72.7% ($n = 3$; $P = 0.002$) and 57.7% ($n = 3$; $P = 0.043$), respectively, indicating that SLIT2 effects did not depend on the mode of ectopic expression. Furthermore, SLIT2-conditioned medium from MiaPaCa$^{TR\text{-}SLIT2}$ clones impaired migration of ROBO1-competent wild-type MiaPaCa, but not of ROBO1-deficient ASPC1 cells (Fig. 2H and I). Use of a purified N-terminal fragment of SLIT2 also reproduced the effects of SLIT2-conditioned tumor cell media (Supplementary Fig. S2E and S2F), and coincubation with a soluble Fc-coupled ROBO1 receptor (ROBO1-Fc) prevented the inhibition of migration (Fig. 2H and Supplementary Fig. S2E). Finally, migration of DANG cells with endogenous SLIT2 expression was enhanced by knockdown of ROBO1 (Fig. 2J and K). Overall, these data are consistent with a ROBO1-mediated, auto/paracrine action of SLIT2 as a suppressor of PDAC cell motility.

Published OnlineFirst January 21, 2014; DOI: 10.1158/0008-5472.CAN-13-1012

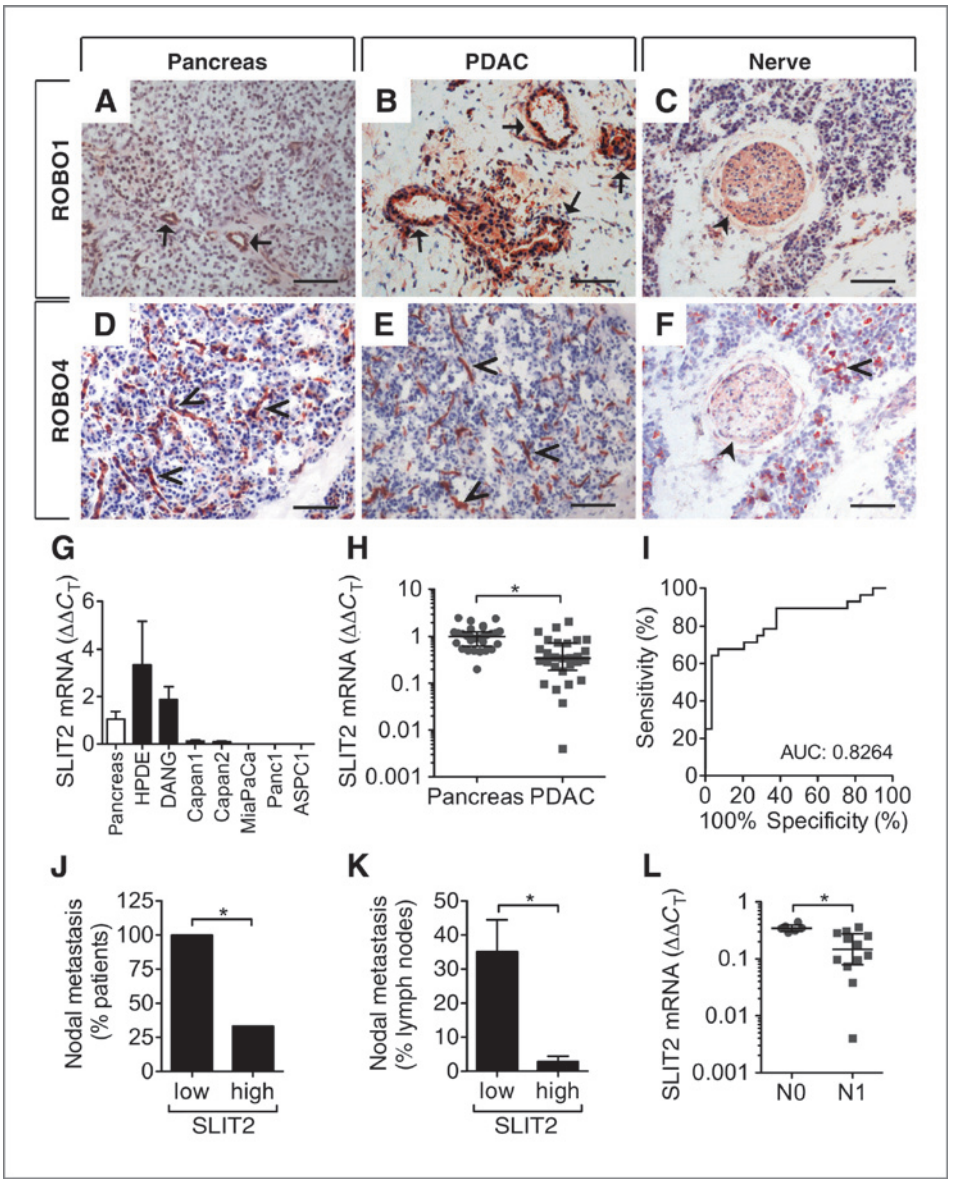

Figure 1. SLIT2 mRNA expression is reduced in human PDAC and inversely correlates with lymph node metastasis. A–F, immunohistochemistries for ROBO1 (A–C) and ROBO4 (D–F) in nontransformed pancreas, PDAC, and intrapancreatic nerves. Arrows, ROBO1 in ductal epithelial cells; arrowheads, ROBO4 in the vasculature; filled arrowheads, pancreatic nerves. Bar, 100 μm. G, SLIT2 mRNA expression in PDAC cell lines using qRT-PCR, normalized to 18S-RNA. H, SLIT2 mRNA expression in PDAC ($n = 28$) and nontransformed pancreas ($n = 29$) was determined using qRT-PCR and normalized to glyceraldehyde-3-phosphate dehydrogenase (GAPDH). Shown is the scatter dot plot with median and interquartile range (H; $P < 0.0001$, Mann–Whitney test). I, receiver-operator characteristic analysis for determination of a cutoff level, which best discriminates PDAC from nontransformed pancreas (cutoff < 0.458, likelihood ratio: 18.64). Further analysis was restricted to tumors exhibiting pathologic SLIT2 mRNA levels ($n = 18$). J–K, incidence of nodal metastasis (J; $P = 0.009$, Fisher exact test) and percentage of tumor-infiltrated lymph nodes (K; $P = 0.005$, Mann–Whitney test) in patients with low (<median, $n = 9$) or high (>median, $n = 9$) tumoral SLIT2 mRNA levels. L, tumoral SLIT2 mRNA levels in patients without (N0) and with nodal metastasis (N1); $P = 0.0043$, Mann–Whitney test. Shown is the scatter dot plot with median and the interquartile range.

SLIT2 exhibits variable effects on endothelial cell migration *in vitro*

Because we detected ROBO receptors in PDAC vasculature, we addressed angioregulatory activities of tumor cell-derived SLIT2 *in vitro*. Use of purified recombinant SLIT2N increased (Fig. 3A), whereas SLIT2-conditioned media from stable MiaPaCa^{SLIT2} clones reduced HUVEC migration (Fig. 3B). Blocking SLIT2 in the MiaPaCa^{SLIT2}-conditioned media by ROBO1-Fc counteracted this effect, suggesting a direct inhibitory action of tumor cell–derived SLIT2 (Fig. 3B). Tumor cell–derived SLIT2, furthermore, impaired VEGF-induced lamellopodia formation of HUVEC by preventing F-actin polymerization and spatial redistribution of cortactin (Fig. 3C–E). Thus, variable direct effects on endothelial motility were observed with purified truncated SLIT2N and PDAC-derived and -processed full-length SLIT2, with the latter exhibiting inhibitory effects.

Published OnlineFirst January 21, 2014; DOI: 10.1158/0008-5472.CAN-13-1012

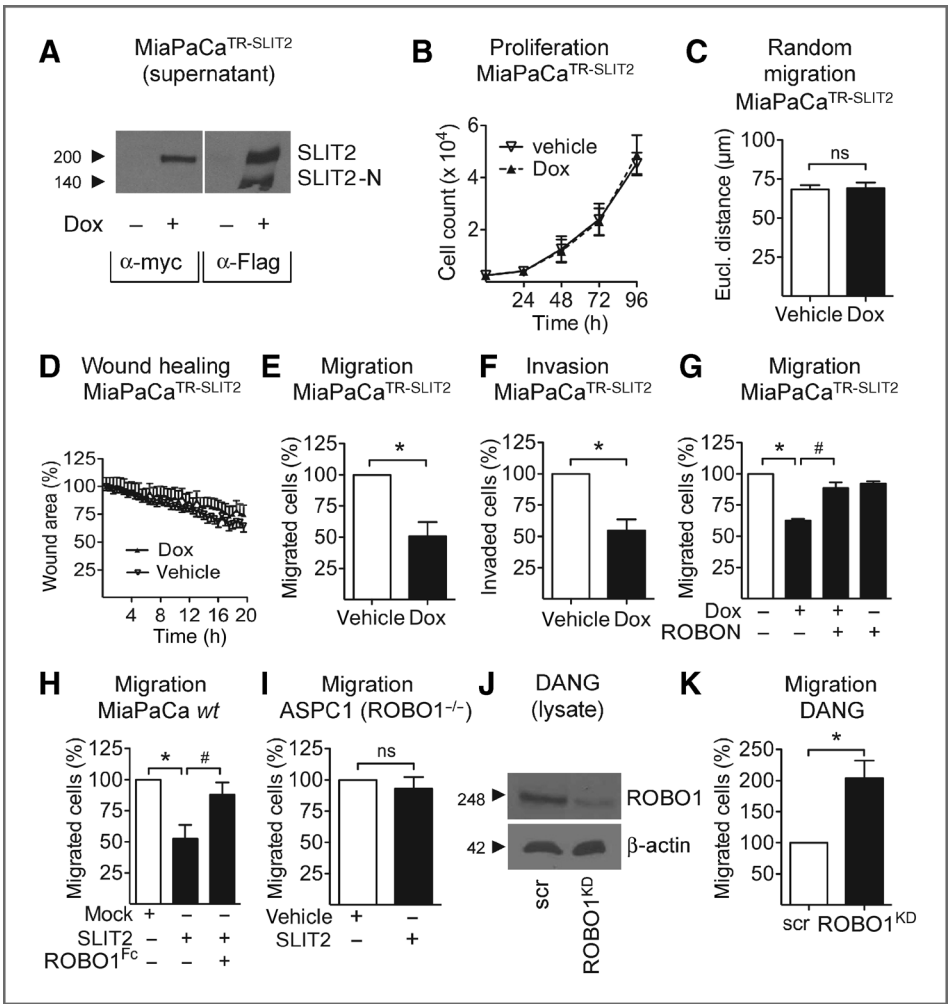

Figure 2. Reexpression of SLIT2 inhibits directed migration and invasion of PDAC cells. A, inducible expression of myc- and Flag-tagged SLIT2 in immunoblots of trichloroacetic acid precipitates from MiaPaCa$^{TR\text{-}SLIT2}$ culture supernatants treated with 1 μg/mL doxycycline (Dox) for 48 hours or vehicle controls. Proteolytic cleavage of full-length SLIT2 (200 kDa) generated the N-terminal SLIT2 fragment (SLIT2-N, 140 kDa). B and C, MiaPaCa$^{TR\text{-}SLIT2}$ cells were treated as above, and cell number was counted ($n = 3$; $P = 0.89$, ANOVA; B) or random migration assessed using time-lapse microscopy. Shown is the Euclidean distance reached at $t = 12$ hours (C; $n = 3$; $P = 0.87$). D, confluent MiaPaCa$^{TR\text{-}SLIT2}$ cell layers were wounded, and percentage reduction of open wound areas evaluated ($n = 3$; $P = 0.37$, ANOVA). E and F, reexpression of SLIT2 inhibited directed migration ($n = 4$; $P = 0.023$) and invasion ($n = 3$; $P = 0.034$) of MiaPaCa$^{TR\text{-}SLIT2}$ cells as compared with vehicle controls. G, ROBON-conditioned medium abrogated the inhibitory effect of SLIT2 on tumor cell migration as compared with mock control medium ($n = 3$; *, $P < 0.001$; #, $P < 0.05$). H and I, SLIT2-conditioned medium from SLIT2-transfected MiaPaCa cells inhibited migration of wild-type (wt) ROBO1-competent MiaPaCa cells (H; $n = 5$; *, $P = 0.013$), but not of ASPC1 cells deficient for ROBO1 (I; $n = 3$; $P = 0.51$), whereas ROBO1-Fc abrogated this effect (H; $n = 5$; #, $P = 0.032$). J and K, shRNA-mediated knockdown of ROBO1 in DANG cells was confirmed using immunoblotting of cell lysates (J) and enhanced migration of DANG cells as compared with scrambled controls (scr; K; $n = 4$; $P = 0.035$), whereas proliferation remained unchanged (not shown).

SLIT2 and ROBO1 inhibit invasion, metastasis, and angiogenesis of PDAC xenografts *in vivo*

To address SLIT2 effects on PDAC growth and progression *in vivo*, MiaPaCa$^{TR\text{-}SLIT2}$ cells were grown as orthotopic xenografts. SLIT2 induction (confirmed in tumor lysates; Supplementary Fig. S4) moderately decreased primary tumor growth (Fig. 4A–C), but substantially reduced abdominal metastasis (Fig. 4D–F) and nodal spread (Fig. 4L), even when size-matched tumors were compared (Supplementary Fig. S5A–S5D). SLIT2 also diminished invasive growth into adjacent organs (Fig. 4J and K). Furthermore, microvessel densities were reduced in MiaPaCa$^{TR\text{-}SLIT2}$ tumors with SLIT2 induction in the overall group (Fig. 4G–I) and in a subgroup analysis of size-matched tumors (Supplementary Fig. S5E and S5F), supporting an antiangiogenic action of SLIT2 *in vivo*.

As high-level SLIT2 production in our overexpression model might not accurately reflect the biologic role of endogenous SLIT2, we pursued a complementary experimental approach and used DANG$^{ROBO1\text{-}KD}$ cells to study the *in vivo* consequences of disrupted SLIT2/ROBO1 signaling in PDAC. DANG$^{ROBO1\text{-}KD}$ tumors exhibited enhanced local invasion and a marked increase in the incidence and extent of metastasis compared with controls, although primary tumor growth was not significantly augmented (Fig. 5A–E and Supplementary Fig. S6A–

Published OnlineFirst January 21, 2014; DOI: 10.1158/0008-5472.CAN-13-1012

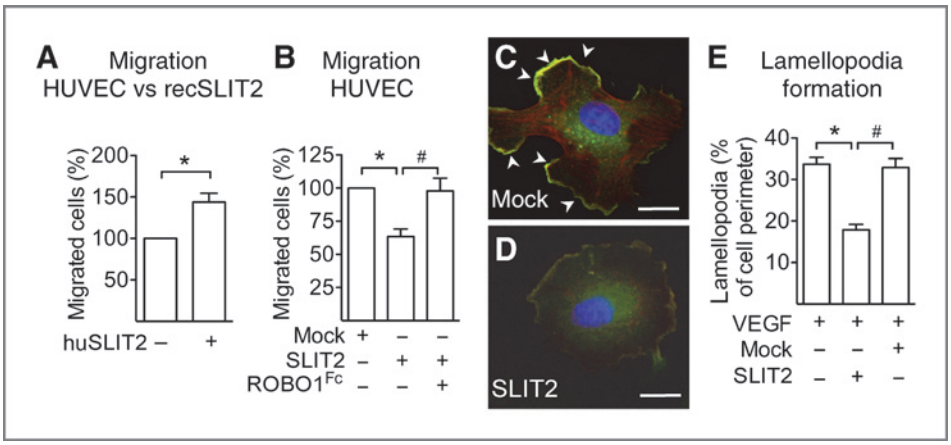

Figure 3. Tumor-derived SLIT2 inhibits migration and lamellopodia formation of endothelial cells. A and B, HUVEC migration toward chemoattractant gradients (2% fetal calf serum, FCS) was evaluated in the presence of recombinant huSLIT2 (A; $n = 4$; $P = 0.027$) or SLIT2- and mock-conditioned media derived from stably transfected MiaPaCa$^{SLIT2/Mock}$ clones, added in the lower Transwell chamber (B; $n = 4$; *, $P = 0.0076$). ROBO1-Fc abrogates effects of SLIT2-conditioned medium (B; $n = 4$; #, $P = 0.021$). C–E, cortactin (green) and phalloidin (red) immunofluorescence illustrated VEGF-induced (50 ng/mL; 1 hour) formation of lamellopodia (C; arrowheads), which was abrogated by SLIT2-conditioned medium (D). Lamellopodia were quantified as percentage of total HUVEC perimeter. A total of $n = 95$–120 individual endothelial cells out of three independent experiments were analyzed (E; $P < 0.0001$, ANOVA). Scale bar, 10 μm.

S6D). Similarly, tumor vascularization was not different between experimental groups—consistent with unaltered SLIT2 levels in this approach (Fig. 5F and Supplementary Fig. S6E and S6F). To interrogate the role of SLIT2 for angiogenesis, we used subcutaneous DANG xenografts, as this approach allowed us to sequester and inactivate SLIT2 by coinjection of ROBO1-Fc. As in the orthotopic setting, DANG^{scr} and DANG$^{ROBO1\text{-}KD}$ tumors presented equal microvessel densities (Supplementary Fig. S7), suggesting that auto/paracrine SLIT2–ROBO1 signaling events in the tumor cells had no major impact on vascularization. In contrast, functional inactivation of SLIT2 by ROBO1-Fc increased vascularization (Supplementary Fig. S7), thus supporting an antiangiogenic role of SLIT2 via interaction with stromal cells.

SLIT2 inhibits invasion and metastasis of syngeneic Panc02 pancreatic cancer *in vivo*

To corroborate the antitumor action of SLIT2 in an immunocompetent model, syngeneic orthotopic Panc02 tumors were evaluated. Primary tumor growth was comparable in mice bearing Panc02^{SLIT2} tumors with ectopic SLIT2 expression as compared with mock controls (Supplementary Fig. S8A–S8C). However, invasive growth into adjacent organs as well as abundance of abdominal metastasis and malignant ascites were markedly diminished in mice bearing SLIT2-producing Panc02^{SLIT2} tumors (Supplementary Fig. S8D–S8H). Thus, antimetastatic and antiinvasive properties of SLIT2 were not confined to immunocompromised xenografts.

SLIT2 inhibits bidirectional chemoattraction of PDAC and neuronal cells

Given that ROBO1 expression was observed in pancreatic nerves, we addressed SLIT2 effects on the mutual interaction of PDAC cells with neuronal cells. Because xenograft tumors are poorly innervated, we combined *in vitro* and *ex vivo* approaches with increasing complexity. First, directed migration of MiaPaCa$^{TR\text{-}SLIT2}$ or Panc1$^{TR\text{-}SLIT2}$ cells toward chemoattractant stimuli from Schwann-cell cultures was diminished by SLIT2 (Fig. 6A and Supplementary Fig. S2G). Vice versa, directed migration of Schwann-cells was reduced, when SLIT2-expressing MiaPaCa$^{TR\text{-}SLIT2}$ cells were grown in the lower chamber (Fig. 6B). Thus, SLIT2 counteracted bidirectional chemoattraction between neuronal and PDAC cells.

SLIT2 impairs unidirectional migration of PDAC cells along nerves

To obtain a representation of tumor cell migration along neurites, coculture assays of DRG and PDAC cell colonies were established (Fig. 6C). Time-lapse microscopy captured the dynamic process by which neurites grew out from DRGs and projected into cancer cell colonies; reciprocally, tumor cells dissociated from the colony, unidirectionally migrated along the neurites, once contact was established, and ultimately formed tumor cell protrusions toward the ganglia of origin (Fig. 6D–F; Supplementary Video S1 and S2). GFP-labeled MiaPaCa cells confirmed that these were tumor cell projections (Supplementary Fig. S9). Under vehicle-control conditions, this neural invasion consistently occurred and increased over time (Fig. 6G). Induction of SLIT2, however, diminished the extent of neural invasion of MiaPaCa$^{TR\text{-}SLIT2}$ cells (Fig. 6G).

Furthermore, evaluation of individually tracked MiaPaCa$^{TR\text{-}SLIT2}$ cells revealed that tumor cells with nerve contact traveled greater distances with increased directness, and reached higher velocities, as compared with cells without nerve contact, which exhibited random, nondirectional movements (Fig. 7). Notably, induction of SLIT2 in MiaPaCa$^{TR\text{-}SLIT2}$ cells with nerve contact impaired their capacity to migrate along neurites by reducing their travel speed and distance, and directionality (Fig. 7I–L). In contrast, SLIT2 did not change these parameters in tumor cells lacking nerve contact

Published OnlineFirst January 21, 2014; DOI: 10.1158/0008-5472.CAN-13-1012

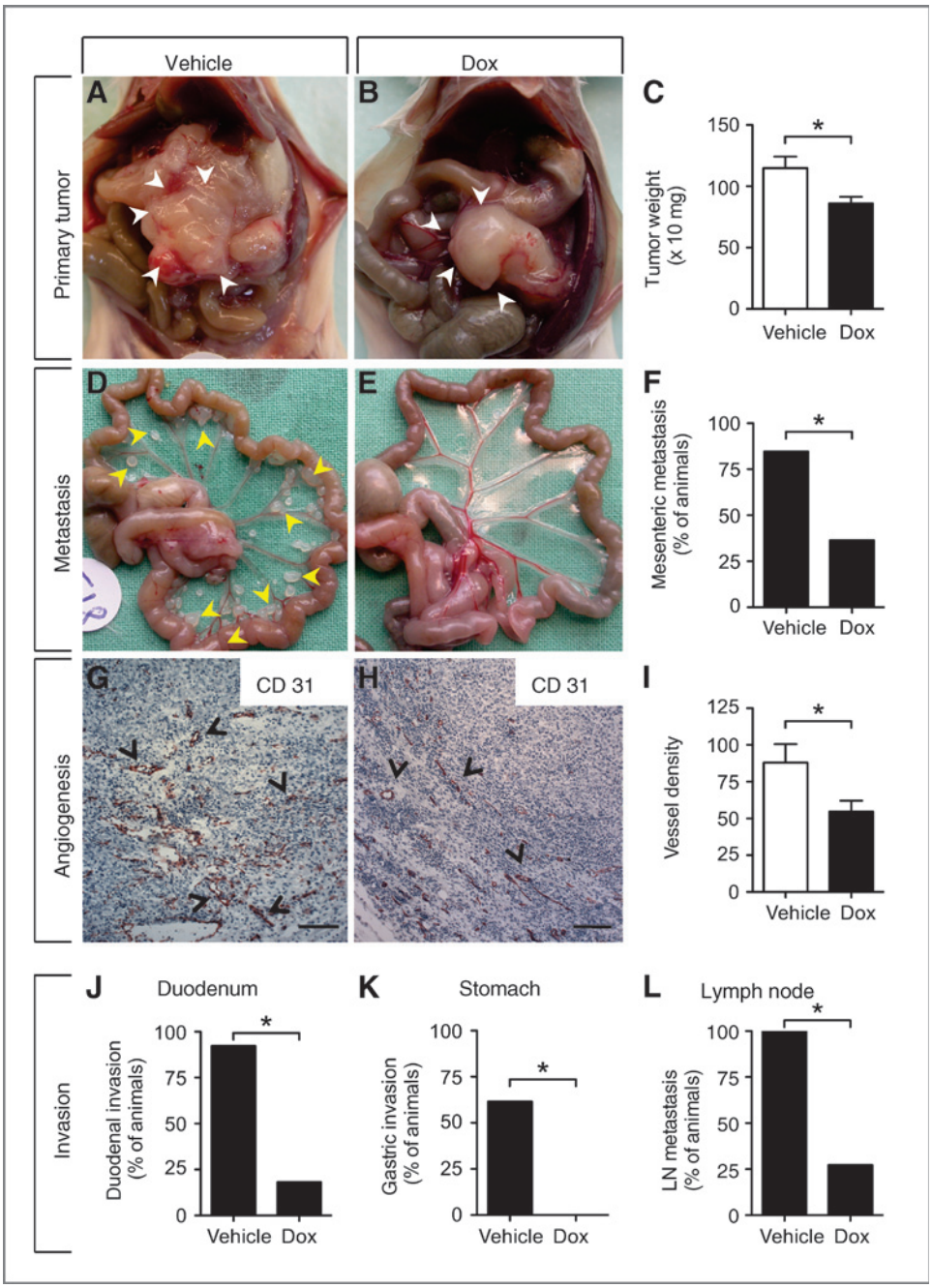

Figure 4. Inducible reexpression of SLIT2 inhibits invasion, metastasis, and angiogenesis of orthotopic pancreatic tumors. A–F, MiaPaCa$^{TR\text{-}SLIT2}$ cells were grown as orthotopic tumors in mice treated with vehicle ($n = 13$) or doxycycline (Dox: 2 mg/mL; $n = 11$) via drinking water. Shown are illustrations of pancreatic tumors *in situ* (A and B; white arrowheads) and excised mesenteries with metastases (D and E; yellow arrowheads) from vehicle or doxycycline-treated mice. C, evaluation of tumor weight; $P = 0.018$, Mann–Whitney test. F and J–L, contingency graphs of mesenteric metastasis (F; $P = 0.033$), tumor invasion into duodenum (J; $P = 0.0005$) and stomach (K; $P = 0.002$), and metastatic spread to retroperitoneal lymph nodes (L; $P = 0.0002$, all Fisher exact test). G–I, CD31^{+} microvessel densities in vehicle (G; $n = 12$) and doxycycline-treated (H; $n = 11$) tumors were quantified (I; $P = 0.036$). Arrowheads, tumor vessels. Scale bar, 200 μm.

(Fig. 7I–L), suggesting that SLIT2 specifically regulated PDAC cell motility in close vicinity with nerves. Overall, these data indicate that SLIT2 inhibits directed navigation of PDAC cells along contacted neurites.

Discussion

Understanding the molecular basis of the almost inevitable, therapy-refractory progression of PDAC constitutes a central task for translational research. A recent sequencing effort in PDAC revealed an unexpected cluster of alterations in genes of the axon guidance factor family (33). More specifically, genomic mutations in the SLIT2 and ROBO1/2 pathway were prevalent, and reduced expression of components of this pathway correlated to shorter survival in PDAC (33). Our current data confirm reduced SLIT2 mRNA expression in PDAC tissues, and delineate the function of SLIT2–ROBO signaling for several clinically relevant aspects of PDAC biology. Main findings in PDAC cells with experimental reexpression of SLIT2 are a reduced capacity to metastasize and to induce neovascularization. Conversely, enhanced invasion, metastasis, and vascularization characterize PDAC xenografts

Published OnlineFirst January 21, 2014; DOI: 10.1158/0008-5472.CAN-13-1012

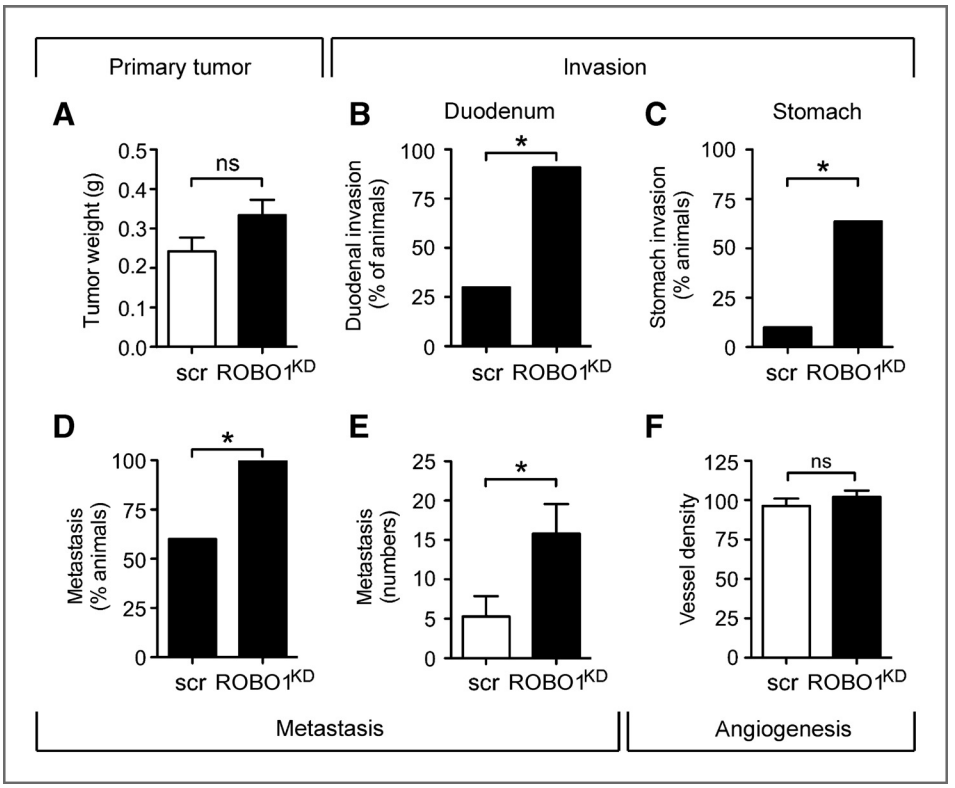

Figure 5. ROBO1-knockdown enhances invasion and metastasis of orthotopic pancreatic tumors. A–E, orthotopic tumors derived from DANG$^{ROBO1\text{-}KD}$ cells ($n = 11$) and scrambled controls (scr; $n = 10$) were evaluated for tumor weight (A; $P = 0.17$). Contingency graphs show incidence of tumor invasion into duodenum (B; $P = 0.0075$) and stomach (C; $P = 0.024$), and lymphatic metastasis (D; $P = 0.035$; all Fisher exact test). Number of metastases per mouse increased in DANG$^{ROBO1\text{-}KD}$ tumor-bearing animals (E; $P = 0.016$, Mann–Whitney test). F, CD31^{+} microvessel density in DANG$^{ROBO1\text{-}KD}$ tumors versus scrambled controls ($P = 0.323$).

with ROBO1 knockdown or sequestration of endogenous SLIT2. The SLIT2-mediated control of tumor spread in our experimental models translates to the clinical observation that low tumoral SLIT2 mRNA levels correlated to nodal spread of PDACs. Our *in vitro* data, furthermore, assign a novel function to SLIT2, as they implicate SLIT2 in the control of pancreatic cancer cell invasion along outgrowing neurites.

Published expression arrays indicate expression of SLIT2 in ductal epithelial cells of the healthy pancreas (34, 35), which fits our detection of SLIT2 mRNA expression in nontransformed pancreas and ductal HPDE cells. We, furthermore, found ROBO4 in the (neo)vasculature, whereas ductal epithelial cells and intrapancreatic nerves displayed ROBO1 immunoreactivity. These observations suggest that SLIT2–ROBO signaling occurs physiologically in the pancreas, which is in line with the reported chemorepellent function of SLIT2 in epithelial differentiation and ductal morphogenesis during breast, lung, colon, and kidney development (20–22). In turn, loss of SLIT2 resulted in deregulated morphogenesis and aberrant epithelial growth in lung and breast cancer (10), which agrees with the current observation of reduced SLIT2 mRNA expression in PDAC. Moreover, the concept of SLIT2 as a tumor suppressor in PDAC is supported by the frequent loss of SLIT2 expression in PDAC cell lines (33, 34).

Our experimental reexpression of SLIT2 in PDAC cells inhibited directed migration and invasion via ROBO1-mediated auto/paracrine mechanisms. These observations are in line with existing concepts on how loss of SLIT2 affects tumor progression, which propose that SLIT2 counteracts cell motility induced by chemoattractant stimulation via cytokines or growth factors (36–38). Different from the SLIT2 mode of action in breast (39) and lung cancer cells (40), we did not detect a SLIT2-dependent regulation of AKT activity in PDAC cells (data not shown), suggesting a cell type–specific wiring of downstream signals.

Three orthotopic *in vivo* models in our study emphasized the capacity of SLIT2/ROBO1 signals to reduce metastatic spread and local invasive growth. This aspect is reflected in the clinical situation, as low SLIT2 mRNA in PDAC specimens was associated with higher incidence and a higher extent of lymph node metastasis. Fittingly, published expression profiles of PDAC specimens with or without lymph node metastasis listed SLIT2 among genes with reduced expression in lymph node–positive PDAC (41).

The SLIT2-mediated suppression of tumor spread in our *in vivo* models may arise from reduced tumor cell motility, and/or as a consequence of impaired tumor angiogenesis. In fact, the enhanced tumor spread in our DANG orthotopic xenografts with ROBO1 knockdown suggests that altered auto/paracrine SLIT2–ROBO1 signaling in tumor cells is sufficient for this phenotype.

Although effects of SLIT2 on angiogenesis in two PDAC models indicated an antiangiogenic action, *in vitro* observations suggest a more complex situation. Intriguingly, purified SLIT2N from commercial sources stimulated endothelial cell migration, whereas SLIT2 produced by PDAC cells inhibited the process, creating a need for further investigation. Explanations are speculative at this time: (i) cofactors produced by PDAC cells possibly account for the inhibitory outcome, which fits the observation that both purified SLIT2N and tumor-

Published OnlineFirst January 21, 2014; DOI: 10.1158/0008-5472.CAN-13-1012

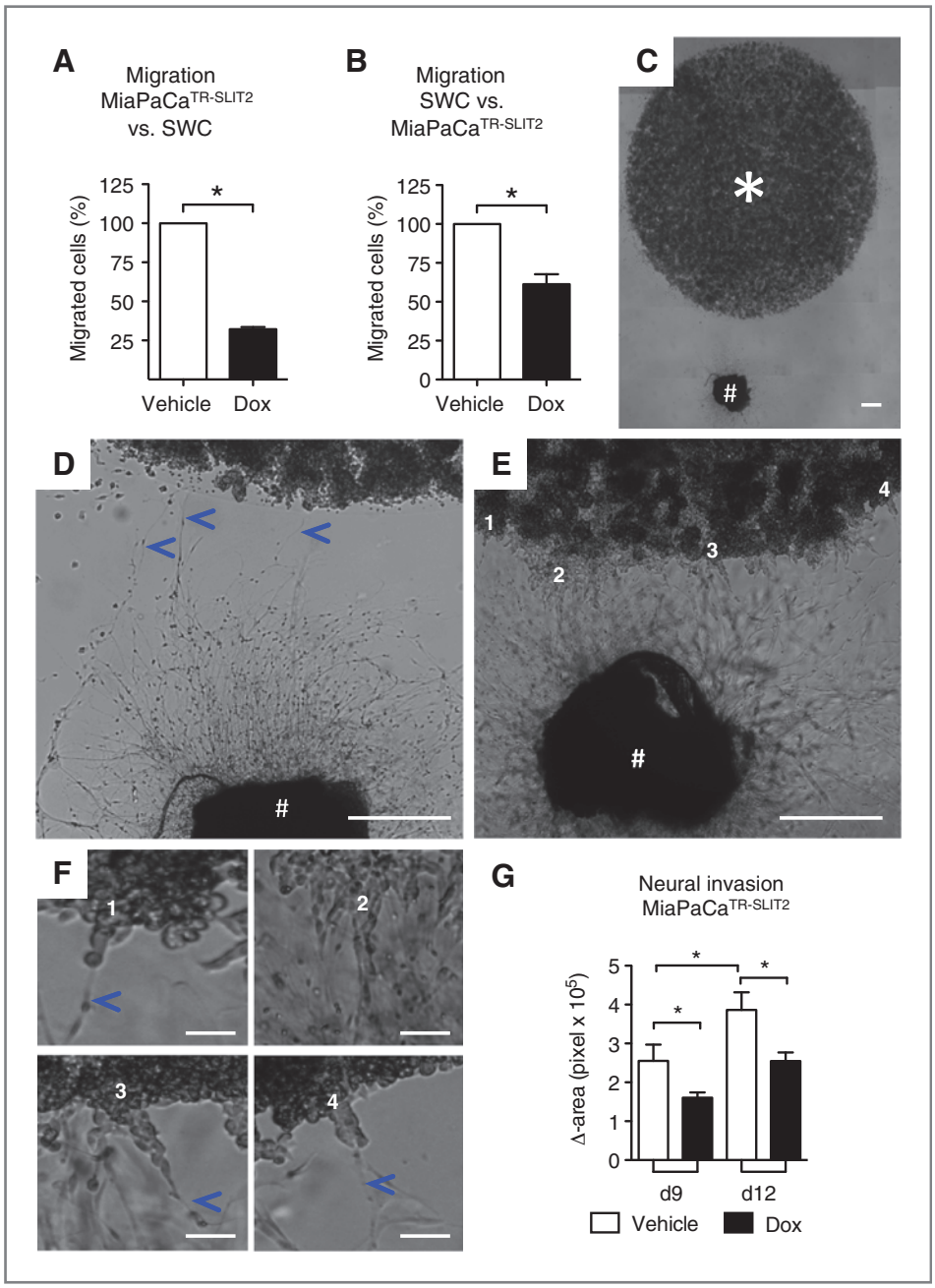

Figure 6. SLIT2 impairs bidirectional chemoattraction of tumor and neuronal cells and inhibits neural invasion in tumor cell–DRG cocultures. A, SLIT2 inhibits migration of MiaPaCa$^{TR\text{-}SLIT2}$ cells toward chemoattractants from Schwann cells (SWC) seeded in the lower Transwell chamber ($n = 3$; $P = 0.014$). B, SLIT2 released from MiaPaCa$^{TR\text{-}SLIT2}$ cells (lower Transwell chamber) inhibits migration of Schwann cells ($n = 3$; $P = 0.027$). C, three-dimensional cocultures of tumor cells (*) and DRG (#) were assembled in Matrigel. D, outgrowth and extension (blue arrowheads) of neurites from the DRG toward the tumor cell colony around day 5. E and F, upon contact, tumor cells disengage and navigate along the contacted neurites (blue arrowheads) toward DRG. Numbers indicate sites of neurite–tumor cell contact initiation and refer to corresponding magnified areas in F. G, neural invasion of vehicle or doxycycline-treated MiaPaCa$^{TR\text{-}SLIT2}$ cells was quantified as the change in area covered by tumor cell projections at day 9 and 12 as compared with the day of coculture start; $n = 3$; *, $P < 0.05$. Scale bars, 500 μm (C–E) or 50 μm (F).

derived SLIT2 preparations uniformly inhibit PDAC cell migration. Precedence for such a cofactor-dependent switch in SLIT2 action was reported with respect to Ephrin-A1 or matrix components (32, 42, 43). (ii) Purified SLIT2N preparations contain but the N-terminal fragment, which binds and activates ROBO1/2 receptors. In contrast, supernatants from PDAC cells contain full-length SLIT2 and the full range of processing products. As full-length SLIT2 may act antagonistic to SLIT2N (32, 42) the differential action of cleavage fragments is a possibility that we actively investigate. (iii) Endothelial cells also express ROBO4 receptors, raising the possibility that the differential repertoire and activation of ROBO4 versus ROBO1/2 determines the migratory response. Published data from siRNA knockdown of either ROBO4 or ROBO1 in lung HMVECs indicate that SLIT2N blunted the VEGF-induced migration of these cells via ROBO4, but not ROBO1 (44).

Reports on SLIT2 effects in the even more complex situation of *in vivo* angiogenesis also offer disparate findings. According to genetic loss-of-function studies, ROBO4 activation via SLIT2 counteracted VEGF-induced vascular leak, whereas disruption of SLIT2–ROBO4 signaling stimulated pathologic angiogenesis and vessel leakiness (45, 46). Other reports have, however, suggested a prometastatic and proangiogenic function of SLIT2 on experimental tumor growth (10, 23, 47, 48). Future,

Published OnlineFirst January 21, 2014; DOI: 10.1158/0008-5472.CAN-13-1012

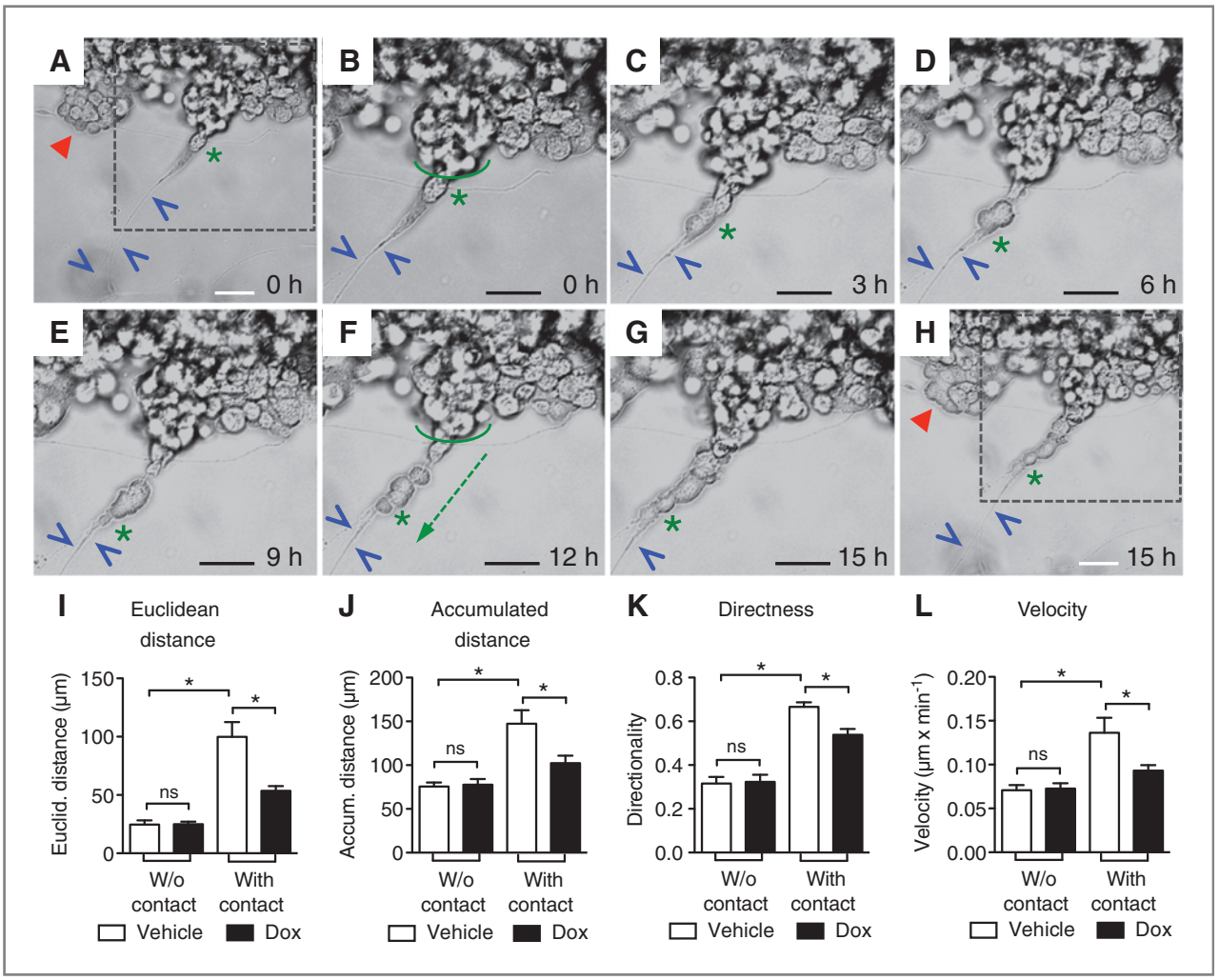

Figure 7. SLIT2 inhibits tumor cell migration along neurites in three-dimensional tumor cell–DRG cocultures. A–H, time-lapse microscopy monitored migration of individual MiaPaCa$^{TR\text{-}SLIT2}$ cells along a contacted DRG neurite. Phase-contrast images depict projection of a DRG neurite (blue arrowheads) into the tumor cell colony and consecutive migration of tumor cells (green asterisk) alongside the neurite. Green arrow (F) indicates the trajectory and migration distance of one individual tumor cell after 12 hours. Migration of tumor cells without nerve contact is illustrated by red arrowheads in A and H. B and G display magnified views of boxed areas in A and H. Scale bar, 50 µm. I–L, trajectories of tumor cells with or without neurite contact were captured, and Euclidian and accumulated distances, directionality, and velocity were quantified. Bar graphs are from 10 experiments with a total number of $n = 45–81$ individually tracked tumor cells per condition; $P < 0.05$, ANOVA.

more detailed understanding of SLIT2/ROBO signaling will hopefully fit these experimental data to a unified concept.

Notably, our studies identified a novel, critical function of SLIT2 for the interaction of PDAC cells with peripheral nerves. Reexpression of SLIT2 in PDAC cells impaired their capacity to navigate along contacted neurites. In comparison, no effect on the movements of tumor cells without neurite contact was apparent, suggesting that SLIT2 counteracted mechanisms that facilitate directional mobility of tumor cells in the immediate vicinity and/or created by contacting nerves. In conjunction with the inhibitory effects of SLIT2 on the migration of PDAC cells against chemoattractant gradients released by neuronal cells in Transwell assays, we assume that both mechanisms, i.e., chemoattraction and contact cues, can contribute.

Currently, we are unable to address SLIT2 function in neural invasion in our xenograft models, which display poor innervation. However, we observed ROBO1 immunoreactivity in pancreatic nerves of human PDAC. During development, the spatial-temporal expression of SLIT2–ROBO1 guidance cues help to confine the patterned migration of those neural crest cells, which give rise to the enteric and sensory neuronal network innervating the pancreas (17, 49). Mechanistically, SLIT2 expressed from tissues adjacent to the trajectory routes provide guidance by repelling ROBO1-expressing neural crest cells and preventing them from entering regions with high concentrations of SLIT2. In analogy to this developmental role, SLIT2 and ROBO1 may conceivably restrict peripheral innervation of the adult pancreas by guiding and/or counteracting growth factor and chemokine-mediated attraction of

pancreatic nerves. In support of a role for axon guidance molecules in the correct growth and patterning of peripheral nerves during organ innervation, loss-of-function studies implicated SLIT2–ROBO1 repulsion in axon fasciculation of motor neurons during muscle innervation (50). In PDAC, silencing of SLIT2 in epithelial tumor cells may possibly relieve repulsion between pancreatic nerves and surrounding tissues and consequently facilitate neural invasion. Our *in vitro* data support this scenario by demonstrating swift movement of PDAC cells along axons, which is impaired by SLIT2 reexpression. Definitive evidence awaits future studies.

Taken together, our results provide evidence that SLIT2 functions as a suppressor of metastasis and local tumor spread in experimental models of PDAC. Mechanistically, tumor cell–derived SLIT2 reduced the motility of PDAC and endothelial cells toward chemoattractants, and, furthermore, prevented PDAC cells from efficient directional movement along conduits provided by axonal projections from cultured ganglia. These experimental findings are reflected in our clinical observation of more extensive nodal metastasis in PDAC with low SLIT2 mRNA. Our data thus emphasize the importance to further assess the Slit–ROBO pathway activity as potential diagnostic and/or prognostic marker, or as candidate therapeutic target in PDAC.

Disclosure of Potential Conflicts of Interest

No potential conflicts of interest were disclosed.

Authors' Contributions

Conception and design: A. Göhrig, K.M. Detjen, J.Y. Wu, B. Wiedenmann, C. Fischer

Development of methodology: A. Göhrig, G. Hilfenhaus, J. Körner, M. Welzel, C. Fischer

Acquisition of data (provided animals, acquired and managed patients, provided facilities, etc.): A. Göhrig, K.M. Detjen, M. Welzel, R. Schmuck, M. Bahra, B. Wiedenmann, C. Fischer

Analysis and interpretation of data (e.g., statistical analysis, biostatistics, computational analysis): A. Göhrig, K.M. Detjen, G. Hilfenhaus, J. Körner, R. Schmuck, J.Y. Wu, B. Wiedenmann, C. Fischer

Writing, review, and/or revision of the manuscript: A. Göhrig, K.M. Detjen, R. Schmuck, J.Y. Wu, B. Wiedenmann, C. Fischer

Administrative, technical, or material support (i.e., reporting or organizing data, constructing databases): A. Göhrig, M. Welzel, M. Bahra, C. Fischer

Study supervision: K.M. Detjen, C. Fischer

Testing, performing, and interpreting immunohistochemistry and providing images: R. Arsenic

Acknowledgments

The authors thank Andrea Behm, Ines Eichhorn, and Maik Schröder for expert technical assistance.

Grant Support

This work is supported by Wilhelm Sander-Stiftung to C. Fischer, by Sonnenfeld-Stiftung to A. Göhrig, and by Horst Müggenburg Stiftung to B. Wiedenmann. J.Y. Wu is supported by NIH and James S. McDonnell Foundation.

The costs of publication of this article were defrayed in part by the payment of page charges. This article must therefore be hereby marked *advertisement* in accordance with 18 U.S.C. Section 1734 solely to indicate this fact.

Received April 9, 2013; revised December 2, 2013; accepted December 23, 2013; published OnlineFirst January 21, 2014.

References

1. Stathis A, Moore MJ. Advanced pancreatic carcinoma: current treatment and future challenges. Nat Rev 2010;7:163–72.
2. Bapat AA, Hostetter G, Von Hoff DD, Han H. Perineural invasion and associated pain in pancreatic cancer. Nat Rev Cancer 2011;11:695–707.
3. Gil Z, Cavel O, Kelly K, Brader P, Rein A, Gao SP, et al. Paracrine regulation of pancreatic cancer cell invasion by peripheral nerves. J Natl Cancer Inst 2010;102:107–18.
4. Ceyhan GO, Demir IE, Altintas B, Rauch U, Thiel G, Müller MW, et al. Neural invasion in pancreatic cancer: a mutual tropism between neurons and cancer cells. Biochem Biophys Res Commun 2008;374:442–7.
5. Ceyhan GO, Bergmann F, Kadihasanoglu M, Altintas B, Demir IE, Hinz U, et al. Pancreatic neuropathy and neuropathic pain–a comprehensive pathomorphological study of 546 cases. Gastroenterology 2009;136:177–86e1.
6. Tessier-Lavigne M, Goodman CS. The molecular biology of axon guidance. Science 1996;274:1123–33.
7. Carmeliet P, Tessier-Lavigne M. Common mechanisms of nerve and blood vessel wiring. Nature 2005;436:193–200.
8. Chedotal A. Slits and their receptors. Adv Exp Med Biol 2007;621:65–80.
9. Mehlen P, Delloye-Bourgeois C, Chedotal A. Novel roles for Slits and netrins: axon guidance cues as anticancer targets? Nat Rev Cancer 2011;11:188–97.
10. Ballard MS, Hinck L. A roundabout way to cancer. Adv Cancer Res 2012;114:187–235.
11. Brose K, Bland KS, Wang KH, Arnott D, Henzel W, Goodman CS, et al. Slit proteins bind Robo receptors and have an evolutionarily conserved role in repulsive axon guidance. Cell 1999;96:795–806.
12. Ypsilanti AR, Zagar Y, Chedotal A. Moving away from the midline: new developments for Slit and Robo. Development 2010;137:1939–52.
13. Li HS, Chen JH, Wu W, Fagaly T, Zhou L, Yuan W, et al. Vertebrate slit, a secreted ligand for the transmembrane protein roundabout, is a repellent for olfactory bulb axons. Cell 1999;96:807–18.
14. Yuasa-Kawada J, Kinoshita-Kawada M, Wu G, Rao Y, Wu JY. Midline crossing and Slit responsiveness of commissural axons require USP33. Nat Neurosci 2009;12:1087–9.
15. Wu W, Wong K, Chen J, Jiang Z, Dupuis S, Wu JY, et al. Directional guidance of neuronal migration in the olfactory system by the protein Slit. Nature 1999;400:331–6.
16. Jia L, Cheng L, Raper J. Slit/Robo signaling is necessary to confine early neural crest cells to the ventral migratory pathway in the trunk. Dev Biol 2005;282:411–21.
17. Giovannone D, Reyes M, Reyes R, Correa L, Martinez D, Ra H, et al. Slits affect the timely migration of neural crest cells via Robo receptor. Dev Dyn 2012;241:1274–88.
18. Bedell VM, Yeo SY, Park KW, Chung J, Seth P, Shivalingappa V, et al. roundabout4 is essential for angiogenesis *in vivo*. Proc Natl Acad Sci U S A 2005;102:6373–8.
19. Park KW, Morrison CM, Sorensen LK, Jones CA, Rao Y, Chien CB, et al. Robo4 is a vascular-specific receptor that inhibits endothelial migration. Dev Biol 2003;261:251–67.
20. Grieshammer U, Le M, Plump AS, Wang F, Tessier-Lavigne M, Martin GR. SLIT2-mediated ROBO2 signaling restricts kidney induction to a single site. Dev Cell 2004;6:709–17.
21. Macias H, Moran A, Samara Y, Moreno M, Compton JE, Harburg G, et al. SLIT/ROBO1 signaling suppresses mammary branching morphogenesis by limiting basal cell number. Dev Cell 2011;20:827–40.
22. Xian J, Clark KJ, Fordham R, Pannell R, Rabbitts TH, Rabbitts PH. Inadequate lung development and bronchial hyperplasia in mice with a targeted deletion in the Dutt1/Robo1 gene. Proc Natl Acad Sci U S A 2001;98:15062–6.
23. Wang B, Xiao Y, Ding BB, Zhang N, Yuan X, Gui L, et al. Induction of tumor angiogenesis by Slit-Robo signaling and inhibition of cancer growth by blocking Robo activity. Cancer Cell 2003;4:19–29.

Published OnlineFirst January 21, 2014; DOI: 10.1158/0008-5472.CAN-13-1012

24. Dallol A, Da Silva NF, Viacava P, Minna JD, Bieche I, Maher ER, et al. SLIT2, a human homologue of the Drosophila Slit2 gene, has tumor suppressor activity and is frequently inactivated in lung and breast cancers. Cancer Res 2002;62:5874–80.
25. Dallol A, Morton D, Maher ER, Latif F. SLIT2 axon guidance molecule is frequently inactivated in colorectal cancer and suppresses growth of colorectal carcinoma cells. Cancer Res 2003;63:1054–8.
26. Schulz P, Fischer C, Detjen KM, Rieke S, Hilfenhaus G, von Marschall Z, et al. Angiopoietin-2 drives lymphatic metastasis of pancreatic cancer. Faseb J 2011;25:3325–35.
27. Furukawa T, Duguid WP, Rosenberg L, Viallet J, Galloway DA, Tsao MS. Long-term culture and immortalization of epithelial cells from normal adult human pancreatic ducts transfected by the E6E7 gene of human papilloma virus 16. Am J Pathol 1996;148:1763–70.
28. Ouyang H, Mou L, Luk C, Liu N, Karaskova J, Squire J, et al. Immortal human pancreatic duct epithelial cell lines with near normal genotype and phenotype. Am J Pathol 2000;157:1623–31.
29. Fischer C, Jonckx B, Mazzone M, Zacchigna S, Loges S, Pattarini L, et al. Anti-PlGF inhibits growth of VEGF(R)-inhibitor-resistant tumors without affecting healthy vessels. Cell 2007;131:463–75.
30. Schulz P, Scholz A, Rexin A, Hauff P, Schirner M, Wiedenmann B, et al. Inducible re-expression of p16 in an orthotopic mouse model of pancreatic cancer inhibits lymphangiogenesis and lymphatic metastasis. Br J Cancer 2008;99:110–7.
31. Hilfenhaus G, Göhrig A, Pape UF, Neumann T, Jann H, Zdunek D, et al. Placental growth factor supports neuroendocrine tumor growth and predicts disease prognosis in patients. Endocr Relat Cancer 2013;20:305–19.
32. Nguyen Ba-Charvet KT, Brose K, Ma L, Wang KH, Marillat V, Sotelo C, et al. Diversity and specificity of actions of Slit2 proteolytic fragments in axon guidance. J Neurosci 2001;21:4281–9.
33. Biankin AV, Waddell N, Kassahn KS, Gingras MC, Muthuswamy LB, Johns AL, et al. Pancreatic cancer genomes reveal aberrations in axon guidance pathway genes. Nature 2012;491:399–405.
34. Tan AC, Jimeno A, Lin SH, Wheelhouse J, Chan F, Solomon A, et al. Characterizing DNA methylation patterns in pancreatic cancer genome. Mol Oncol 2009;3:425–38.
35. Vincent A, Omura N, Hong SM, Jaffe A, Eshleman J, Goggins M. Genome-wide analysis of promoter methylation associated with gene expression profile in pancreatic adenocarcinoma. Clin Cancer Res 2011;17:4341–54.
36. Stella MC, Trusolino L, Comoglio PM. The Slit/Robo system suppresses hepatocyte growth factor-dependent invasion and morphogenesis. Mol Biol Cell 2009;20:642–57.
37. Marlow R, Strickland P, Lee JS, Wu X, Pebenito M, Binnewies M, et al. SLITs suppress tumor growth *in vivo* by silencing Sdf1/Cxcr4 within breast epithelium. Cancer Res 2008;68:7819–27.
38. Yuasa-Kawada J, Kinoshita-Kawada M, Rao Y, Wu JY. Deubiquitinating enzyme USP33/VDU1 is required for Slit signaling in inhibiting breast cancer cell migration. Proc Natl Acad Sci U S A 2009;106:14530–5.
39. Chang PH, Hwang-Verslues WW, Chang YC, Chen CC, Hsiao M, Jeng YM, et al. Activation of Robo1 signaling of breast cancer cells by Slit2 from stromal fibroblast restrains tumorigenesis via blocking PI3K/Akt/beta-catenin pathway. Cancer Res 2012;72:4652–61.
40. Tseng RC, Lee SH, Hsu HS, Chen BH, Tsai WC, Tzao C, et al. SLIT2 attenuation during lung cancer progression deregulates beta-catenin and E-cadherin and associates with poor prognosis. Cancer Res 2010;70:543–51.
41. Kim HN, Choi DW, Lee KT, Lee JK, Heo JS, Choi SH, et al. Gene expression profiling in lymph node-positive and lymph node-negative pancreatic cancer. Pancreas 2007;34:325–34.
42. Nguyen-Ba-Charvet KT, Brose K, Marillat V, Sotelo C, Tessier-Lavigne M, Chedotal A. Sensory axon response to substrate-bound Slit2 is modulated by laminin and cyclic GMP. Mol Cell Neurosci 2001;17:1048–58.
43. Dunaway CM, Hwang Y, Lindsley CW, Cook RS, Wu JY, Boothby M, et al. Cooperative signaling between Slit2 and Ephrin-A1 regulates a balance between angiogenesis and angiostasis. Mol Cell Biol 2011;31:404–16.
44. Marlow R, Binnewies M, Sorensen LK, Monica SD, Strickland P, Forsberg EC, et al. Vascular Robo4 restricts proangiogenic VEGF signaling in breast. Proc Natl Acad Sci U S A 2010;107:10520–5.
45. Jones CA, Nishiya N, London NR, Zhu W, Sorensen LK, Chan AC, et al. Slit2-Robo4 signalling promotes vascular stability by blocking Arf6 activity. Nat Cell Biol 2009;11:1325–31.
46. Jones CA, London NR, Chen H, Park KW, Sauvaget D, Stockton RA, et al. Robo4 stabilizes the vascular network by inhibiting pathologic angiogenesis and endothelial hyperpermeability. Nat Med 2008;14:448–53.
47. Schmid BC, Rezniczek GA, Fabjani G, Yoneda T, Leodolter S, Zeillinger R. The neuronal guidance cue Slit2 induces targeted migration and may play a role in brain metastasis of breast cancer cells. Breast Cancer Res Treat 2007;106:333–42.
48. Yang XM, Han HX, Sui F, Dai YM, Chen M, Geng JG. Slit-Robo signaling mediates lymphangiogenesis and promotes tumor lymphatic metastasis. Biochem Biophys Res Commun 2010;396:571–7.
49. De Bellard ME, Rao Y, Bronner-Fraser M. Dual function of Slit2 in repulsion and enhanced migration of trunk, but not vagal, neural crest cells. J Cell Biol 2003;162:269–79.
50. Jaworski A, Tessier-Lavigne M. Autocrine/juxtaparacrine regulation of axon fasciculation by Slit-Robo signaling. Nat Neurosci 2012;15:367–9.